



HAL
open science

Arrays of high aspect ratio magnetic microstructures for large trapping throughput in lab-on-chip systems

Samir Mekkaoui, Damien Le Roy, Marie-Charlotte Audry, Joël Lachambre, Véronique Dupuis, Jérôme Desgouttes, Anne-Laure Deman

► To cite this version:

Samir Mekkaoui, Damien Le Roy, Marie-Charlotte Audry, Joël Lachambre, Véronique Dupuis, et al.. Arrays of high aspect ratio magnetic microstructures for large trapping throughput in lab-on-chip systems. *Microfluidics and Nanofluidics*, 2018, 22 (10), pp.119. 10.1007/s10404-018-2141-6 . hal-02326961

HAL Id: hal-02326961

<https://hal.science/hal-02326961v1>

Submitted on 22 Oct 2019

HAL is a multi-disciplinary open access archive for the deposit and dissemination of scientific research documents, whether they are published or not. The documents may come from teaching and research institutions in France or abroad, or from public or private research centers.

L'archive ouverte pluridisciplinaire **HAL**, est destinée au dépôt et à la diffusion de documents scientifiques de niveau recherche, publiés ou non, émanant des établissements d'enseignement et de recherche français ou étrangers, des laboratoires publics ou privés.

Arrays of high aspect ratio magnetic microstructures for large trapping throughput in Lab-On-Chip systems

Samir Mekkaoui¹, Damien Le Roy², Marie-Charlotte Audry¹, Joël Lachambre³, Véronique Dupuis², Jérôme Desgouttes¹, Anne-Laure Deman¹

¹ Institut des Nanotechnologies de Lyon INL-UMR5270, CNRS, Université Lyon 1, Villeurbanne F-69622, France

² Institut Lumière Matière ILM-UMR 5306, CNRS, Université Lyon 1, Villeurbanne F-69622, France Laboratoire

³ Laboratoire Matériaux, Ingénierie et Sciences (MATEIS), INSA-Lyon, CNRS, UMR 5510, 20 Av. Albert Einstein, 69621 Villeurbanne, France

Corresponding author: Samir Mekkaoui, samir.mekkaoui@univ-lyon1.fr

ORCID: 0000-0002-9898-4495

Abstract

Here we report a novel technology that requires simple fabrication process, to obtain highly efficient magnetic micro-traps. Developed micro-traps consist in chains of iron particles diluted in PolyDiMethylSiloxane (PDMS). X-ray tomography was used to analyze the microstructure of particle ordering in the PDMS membrane and revealed the predominance of chain-like agglomerates. Largest formed traps, with diameter ranging from 4 to 11 μm are found to be the most efficient. The self-organized trap arrays are characterized by a density of 1300 magnetic microtraps/ mm^2 , with an average nearest neighbour distance, center-to-center, of 21 μm . Implemented in a microfluidic channel operating at a flow rate of 3 mL/h - a fluid flow of 8,3 mm/s - we measured trapping throughputs up to 7100 beads/min with an average distribution of 750 beads/ mm^2 . At fluid velocity up to 9,7 mm/s a trapping efficiency of 99,99% were measured. This novel technology allows to trap thousands of beads with throughputs that permit to compete with hydrodynamic trapping functions, while requiring simple fabrication process, and handling.

1 Introduction

Lab on a chip (LOC) technology brings numerous benefits for biomedical and environmental applications. LOC significantly reduces the amount of biological sample and reagent, the cost and the time of analysis, and it enables individual cell investigations. One of the most appealing potential of LOC is certainly the development of delocalized analysis solutions, performed in laboratories. For biomedical purpose, LOC working principle involves the manipulation of cells or functionalized beads, generally seeking either high throughputs or precise positioning and manipulation of single objects. In this scope, various solutions, including hydrodynamic, optical, dielectrophoretic, magnetic or acoustic actuations were developed. B. Cetin et al. (Cetin et al. 2014) made an extensive comparison of these techniques based on their implementation, microfabrication and materials and their performances, in particular throughput, considering clinical and diagnostic applications. All techniques present advantages or drawbacks that are weighted differently according to the use. When high sorting throughputs are required, hydrodynamic, acoustic and magnetic approaches are the most competitive. Single cell analysis also represents a strong challenge and aroused great interest in the LOC community during the past ten years (Hosic et al. 2015; Narayanamurthy et al. 2017). Indeed, it permits to reveal individual cell characteristics, due to cell-to-cell variation, cell cycle stages, or rare cell event and to access statistics about cells heterogeneity (Hosic et al. 2015; Yesilkoy et al. 2016; Narayanamurthy et al. 2017), hidden in global studies of large population. Similarly, manipulation of single microbeads has attracted a lot of interest recently (Kim et al. 2012; Tekin

1 and Gijs 2013; Xu et al. 2013). Functionalized microbead arrays are indeed powerful tools to
2 detect and quantify biological target (proteins, RNA, DNA, ...) or to trap labeled cells. The
3 hydrodynamic contact-based approach has been widely developed to trap single microbead or
4 cell (Chen et al. 2015; Yesilkoy et al. 2016; Delapierre et al. 2017; Narayanamurthy et al. 2017).
5 Vertical traps such as microwells or lateral traps microfluidics such as U-shaped
6 microstructures or pockets were precisely designed and used for this purpose. V.
7 Narayanamurthy et al. have recently reviewed current achievements in microfluidics
8 hydrodynamic trapping for single cell analysis. Even though this approach presents advantages,
9 notable drawbacks remain. Hydrodynamic methods can require sophisticated fabrication
10 processes owing to trap dimensions, target specific geometries, and in order to minimize fluidic
11 flow disturbances inherent to trap footprints. Dedicated pumping systems and fluidic controls
12 are often needed and add complexity in the device handling.
13
14

15 Magnetic forces can be promising for single objects trapping. This approach is based on
16 *magnetophoresis* which refers to the motion of an object in a non-uniform magnetic field.
17 Magnetophoresis is implemented in Lab On Chip (Dempsey et al. 2007; Li et al. 2011; Rasponi
18 et al. 2011; Forbes and Forry 2012; Marchi et al. 2015), to perform the concentration, separation
19 or trapping of magnetically labelled cells (Yu et al. 2011), deoxygenated red blood cells (Nam
20 et al. 2013), or functionalized magnetic microbeads (Saliba et al. 2010). The magnetic method
21 does not require cumbersome and specialized equipment which could hinder their handling by
22 biological or medical laboratory. Indeed, magnetic forces can be generated by using either a
23 simple external (bulk) permanent magnet (Mohamadi et al. 2015) or by a micrometer-sized
24 magnetic structure nearby or within the microfluidic channel, named micro-magnets
25 (Esmailsabzali et al. 2016). The latter approach permits to obtain larger magnetic field
26 gradients, thus larger magnetic forces (Le Roy et al. 2016b) and to design target-size traps.
27 Literature can be divided into two distinct kinds of micro magnets, made of hard magnetic
28 materials (Dumas-Bouchiat et al. 2010; Arnold and Wang 2009), or soft magnetic materials
29 (Dempsey et al. 2014; Deman et al. 2017; Jung et al. 2010). The first ones, permanently
30 magnetized, work autonomously, but are limited to fixed force and necessitate costly and
31 complex fabrication process, especially because its performances highly depend on the material
32 microstructure (Zanini et al. 2011). The second ones need an external magnet in order to
33 generate a magnetic field but offer the opportunity to easily tune the magnetic force during
34 experiments and imply easier fabrication process. Usually, Ni or permalloy thin films are
35 patterned by lithography to obtain micromagnets of typically 5-100 μ m in size (Chen et al. 2014;
36 Jaiswal et al. 2017; Henighan et al. 2010). These processes still require several manufacturing
37 steps, and face challenges related to the heterogeneous integration of magnetic materials with
38 polymers, mainly PolyDiMethylSiloxane (PDMS), such as tedious alignment procedures (for
39 locating the traps in the channels,) and tightness issues. Micromagnet arrays were reported to
40 work as magnetic tweezers that enable precise manipulation of magnetic beads or cells
41 (Henighan et al. 2010; Rampini et al. 2016), to traps rare cells (Chen et al. 2014) or for single
42 cell analysis (Jaiswal et al. 2017).
43
44
45
46
47
48
49

50 We propose a novel technology to obtain efficient magnetic micro-trap arrays. The traps consist
51 in high aspect ratio agglomerates of magnetic particles diluted in a polymer matrix. The
52 magnetization and magnetic susceptibility are the two key parameters of soft micro-magnets as
53 they determine the maximum reachable force. We have chosen iron to take benefit of its high
54 magnetization. Through the formation of high aspect ratio agglomerates we induced an
55 increased effective magnetic susceptibility (Khashan and Furlani 2014; Le Roy et al. 2016a).
56 This novel technology, inspired by composite-polymer approach (Faivre et al. 2014; Zhou and
57 Wang 2016; Royet et al. 2017), is low cost and requires simple fabrication process that breaks
58 with standard microfabrication approaches. We obtained an array of 1300 magnetic micro-
59
60
61
62
63
64
65

traps/mm², 4 to 11 μm in diameter, spaced with an average nearest neighbour distance, center-to-center, of 21 μm. In this study, we characterized the composite structure using X-ray tomography and Atomic Force Microscopy (AFM). We characterized the trapping performances when implemented in microfluidic channel, with model superparamagnetic beads. Our findings show high efficiency with 99.99% of injected beads trapped at flow rates of 3 and 3.5 mL/h, respectively flow velocities of 8.3 and 9.7 mm/s. We measured throughputs up to 7100 trapped beads/min. Considering the achievable trap size and areal density, these materials could be used for single cell assays. The final part of this report is dedicated to this application, notably assessing the fraction of traps occupied by single objects.

2 Microfabrication technology

2.1 Fabrication of the composite membrane integrating chains of particles

The composite (I-PDMS) was obtained through the mixture of carbonyl iron microparticles (Fe-C dry powder, 0.5-7μm diameter, 97% Fe basis, Sigma-Aldrich) and PDMS elastomer (10/1 ratio of monomer and curing agent, respectively, Sylgard from Samaro) with concentration of 1 wt% and 5 wt%. They were mixed in a mortar for around 4 minutes until obtaining a visually homogeneous material. Fig. 1 shows the fabrication steps. Composite membranes were patterned using 100 μm thick molds made of Kapton film (Adicaz, France), bonded on silanized glass slice. Two sizes of molds were prepared: 10 mm x 10 mm and 10 mm x 30 mm. To create high aspect ratio magnetic agglomerates extended through the composite membrane thickness, a magnetic field was applied during the PDMS reticulation for 3 hours at 70°C (Fig. 1a-b). The magnetic field is created by a pair of permanent magnet of 10 x 11 x 2.5 cm³, spaced of 6 cm. The mold containing the composite was positioned onto one magnet, where a magnetic field of 150 mT was measured using a Keithley Teslameter. The opposite magnet permits to significantly reduce the magnetic field gradient across the composite. At the position of the composite (1 mm from the magnet surface), the magnetic field gradient is of 0.25 T/m, as calculated using Comsol ® simulation tools. After reticulation, the Kapton mold was then removed, leaving a 100 μm thick patterned composite membrane (Fig. 1c). Pure PDMS (10/1 ratio of monomer and cross-linking agent) was poured on the composite, cured at 70°C for 3h, and peeled off from the glass slice to obtain a 2 mm thick PDMS/composite membrane (Fig. 1d-e).

2.2 Device fabrication

We patterned channels in pure PDMS matrix following a conventional soft-lithography process, using 50 μm dry photoresist (Ethertec®) (Fig. 1f-h). Channel dimension was 100 μm thick (two layer of photoresist) and 1000 μm width. We sealed the channel with the as-prepared magnetic membranes using O₂ plasma bonding (Fig. 1i). A schematic of the obtained microdevice is shown on Fig. 1j.

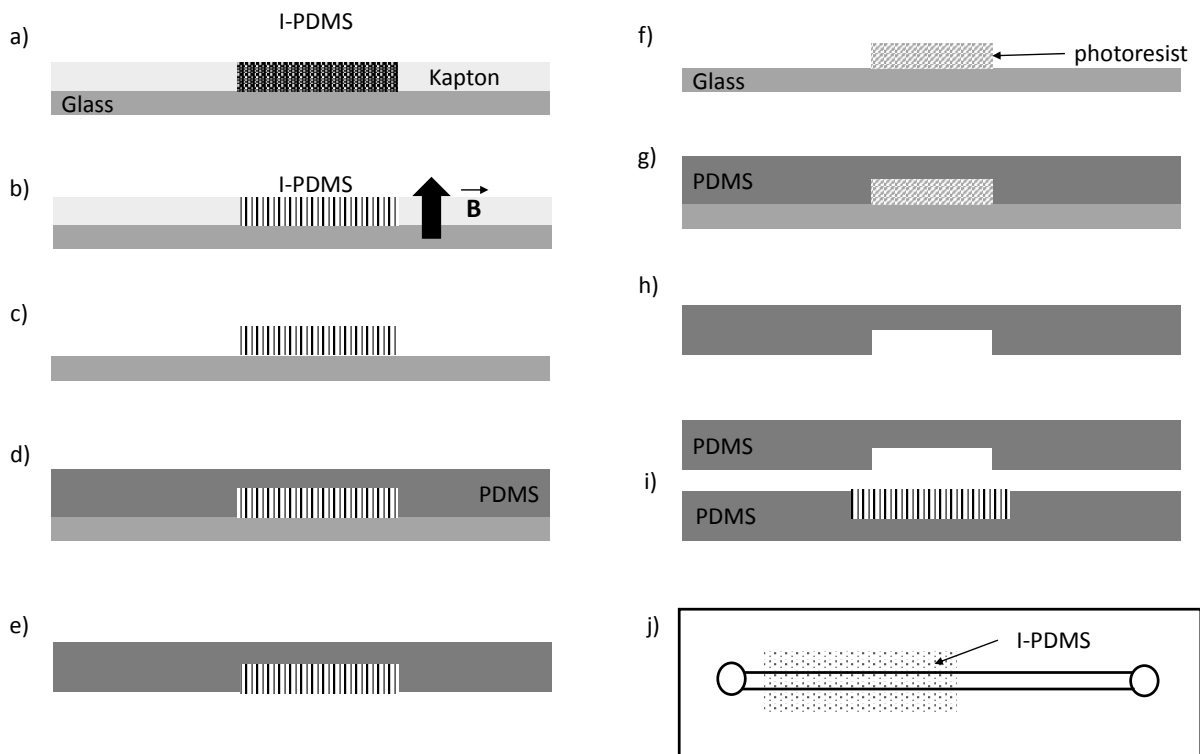


Fig. 1 Fabrication process. **(a)** A Kapton film is patterned on a glass slide and I-PDMS (1 wt% or 5 wt%) is poured in the pattern. A blade is used to remove the excess of composite **(b)** The I-PDMS is cured for 3h at 70°C while being submitted to a vertical magnetic field of $B = 130$ mT, in order to self-organize Fe-C particles in the PDMS matrix **(c)** The Kapton film is removed leaving only the self-organized composite membrane **(d)** PDMS is poured on the membrane, then cured for 3h at 70°C. **(e)** The PDMS/I-PDMS membrane is unmolded. **(f)** The microfluidic channel mold is obtained through photolithography **(g)** PDMS is poured on the mold to replicate the mold and **(h)** unmolded **(i)** O_2 plasma bonding is performed to seal the device comprising the microfluidic channel and the composite membrane. **(j)** is schematic of the device. Dots represent the location of the composite in the device.

2.3 Material and experimental set-up

The inner structure of the composite was characterized using X-ray tomography. These experiments were conducted on 1 wt% and 5 wt% I-PDMS concentration using “EasyTom Nano” μ CT tomograph from “RX Solutions” company. The X-ray source is a LaB6 cathode with a diamond window to allow higher flux (20 μ A) and the used focal spot is 0.25 μ m width knowing that scans are done with a 0.3 μ m voxel size. As Fe-C is quite absorbent, a tension of 90 kV is applied. A CCD detector with a matrix of 2000 x 1312 pixel was used to take projections over 1400 angular positions. After reconstruction, a volume of 1800 x 1100 x 240 vx, i.e. 540 x 330 x 72 μ m³, is obtained. Post treatment are done using ImageJ software in order to get a 3D picture of the sample, but also to extract qualitative results as spatial organization of the particles and quantitative results as effective volume fraction or aspect ratio adopted by those soft structures. Composite topographies were recorded with AFM (Asylum Research MFP-3D) in the tapping mode with silicon probes of nominal radius of curvature 10 nm and nominal spring constant 42 N/m.

Concerning trapping function evaluation in microchannel, superparamagnetic microbeads (12 μ m average diameter, consisting of magnetite nano-inclusions in a polystyrene matrix, Kisker $\text{\textcircled{R}}$) were suspended in a filtered Phosphate Buffered Saline (PBS) (Invitrogen) with a

concentration of 10^3 beads/ μl . During the experiment, the microfluidic channel was positioned on a NdFeB ($6 \times 3 \times 1.5 \text{ cm}^3$). It generated a magnetic field in the channel, i.e. at 2 mm from the magnet surface, of 300 mT (measured using a Keithley Teslameter). Characterization of beads trapping and release was realized using a microscope (Olympus BX51M) and recorded using a camera (Moticam2000, Motic). Obtained images were analyzed using ImageJ® software.

3 Results and discussion

3.1 Composite microstructuration

Under an external magnetic field, carbonyl iron particles can be seen as an ensemble of aligned magnetic dipoles. Before complete PDMS reticulation, the particles are allowed to move within the polymer, and their motion is governed by dipolar interactions and gravity. Adjacent particles are attracted along the flux lines and repelled in the orthogonal directions. These directional interactions lead to the formation of high aspect ratio agglomerates along the flux lines, homogeneously distributed within the matrix. Fig. 2 displays reconstructed 3D profiles from X-ray tomography performed on a volume of $540 \times 330 \times 72 \mu\text{m}^3$. The deduced Fe-C particles size, ranging from 0.5 to $6 \mu\text{m}$, is in good agreement with our SEM (Scanning Electron Microscopy) observations. For both concentrations, 1 wt% and 5 wt%, the tomography images revealed two types of organizations: expected chain-like agglomerates (CA), but also isotropic agglomerates (IA). CA only represent 42% of all agglomerates in both 1 wt% and 5 wt% composites but contain 92% and 96% of the total amount of Fe-C particles, respectively. IA sizes are found to be less than $6 \mu\text{m}$, and mostly localized at the bottom of the membrane (fig 2.b). Since the magnetic field gradient during cross-linking is rather small, 0.25 T/m (calculated using Comsol® simulation tools), we believe that this concentration of IA at the bottom mainly originates from the gravitational force.

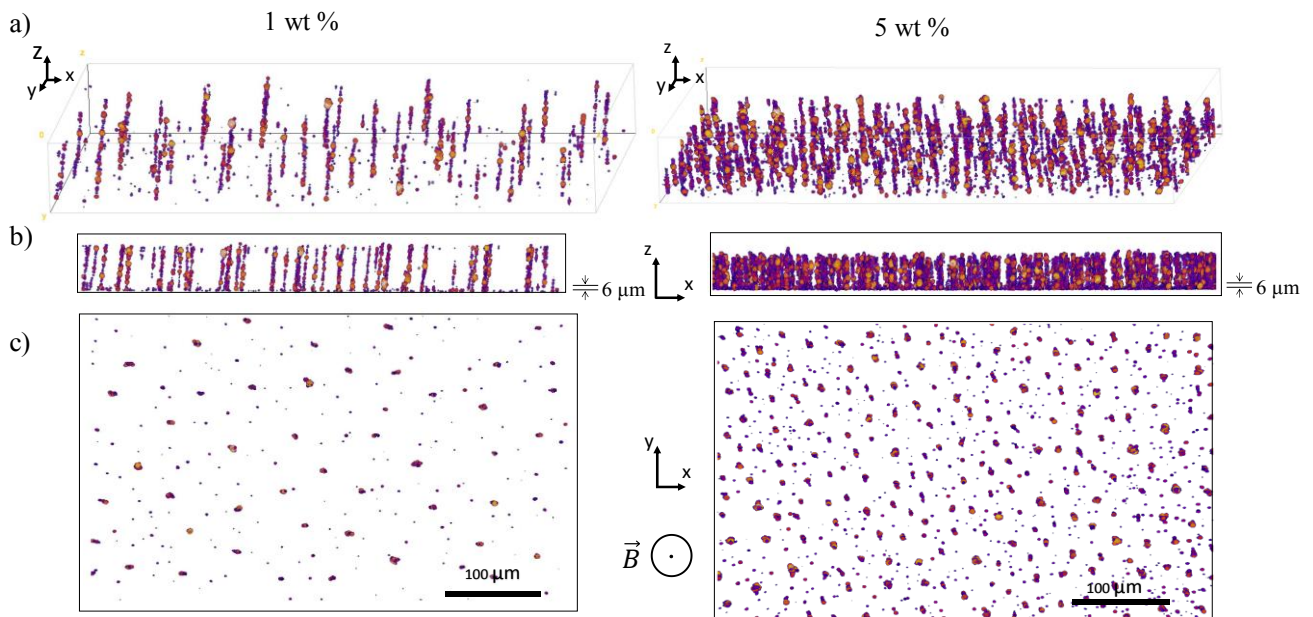


Fig. 2 (a) X-ray tomography reconstruction and projections on (b) XZ plane, bottom of images ($6 \mu\text{m}$ high) cropped in order to remove IA is shown, and (c) XY plane

When implemented into microfluidic devices, these agglomerates locally generate magnetic field gradients and then serve as magnetic traps. Fig. 2c displays top views of the composite membranes, showing the traps distribution. They revealed a non-random organization, which is attributed to dipolar repulsion between the magnetized agglomerates during the preparation. We used AFM to investigate the composites surfaces roughness. The 1 wt% and 5 wt% membranes exhibited an average roughness of 6 nm (50 nm peak-peak) and 13 nm (100 nm peak-peak), respectively. Although the 5 wt% composite is twice as rough as the 1wt% composite surface, it remains relatively smooth as compared to the dimensions of the target objects ($>10\ \mu\text{m}$) (fig.3).

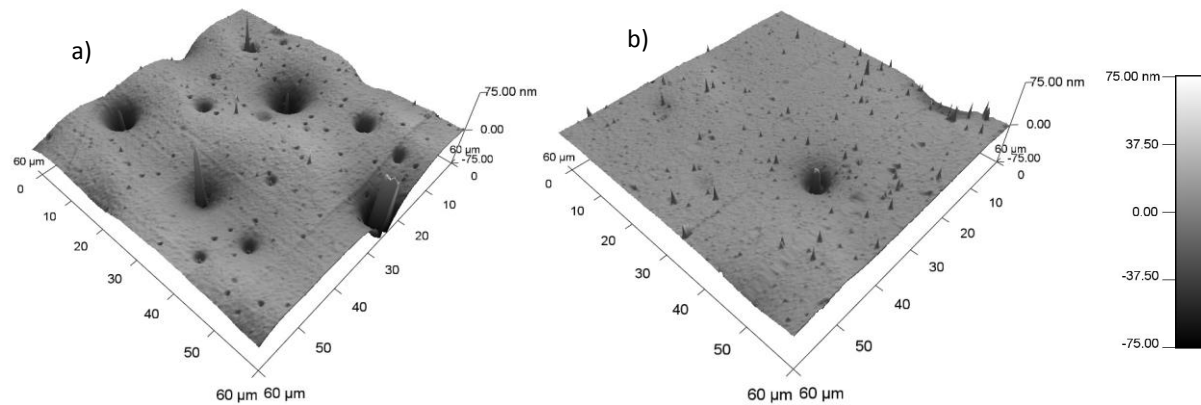


Fig. 3 Surface profile measured with AFM of (a) 5 wt% composite and (b) 1 wt% composite.

We found that 1 wt% and 5 wt% composites are characterized by densities of around 1500 traps/mm and 5000 traps/mm, respectively, without distinction between CA and IA. Fig 4. shows that the distribution of trap diameters exhibits two maxima, centered at 2 and 7 μm in both composite concentrations. In the following discussion, for the sake of simplicity, we will refer to two populations of traps, “small traps” and “large traps”, corresponding both peaks of the size distribution, the discriminating diameter being 4 μm . Small traps are predominant as they represent almost 81% of traps at 1wt% composite and 74% of traps at 5 wt%. To relate the CA and IA structures to the trap size, we reconstructed a new batch of tomography images after cropping a 6 μm -thick superficial layer in the ZX plane of all images, so that to remove IA (Fig. 2b). The resulting cropped images permit to specifically characterize CA structures. Fig. 4a reports the diameter distribution from IA and CA structures for 1 wt% and 5 wt% composite membranes. At 5 wt% the proportion of thicker CA structures is slightly increased, like it has been already observed by other groups (Ghosh and Puri 2013; Günther et al. 2011). Most of IA structures, 94 to 97% for each composite, gave rise to “small traps” as their diameter is inferior to 4 μm . Fig. 4b shows the proportion of traps originating from IA and CA structures based on the discriminating diameter of 4 μm for small and large traps. 90% of large traps observed on the membrane surface originate from CA structures.

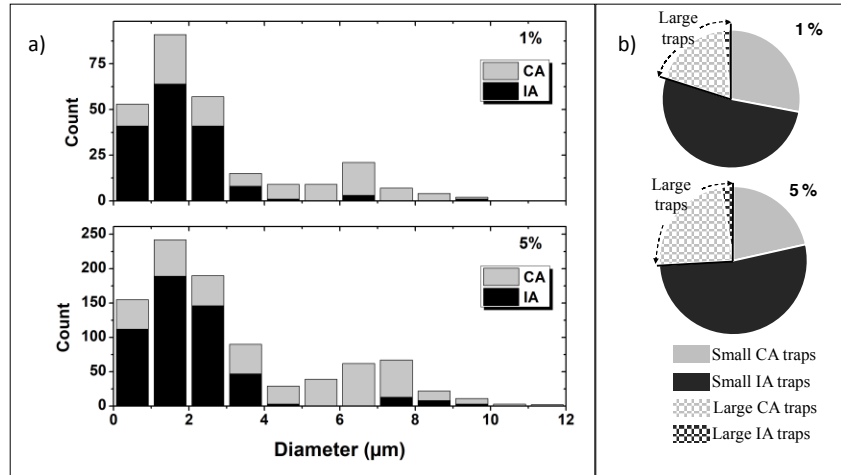


Fig. 4 (a) Distribution of traps diameter of 1 wt% membrane (top) and 5 wt% membrane (bottom), in black the IA proportion and in grey the CA proportion. **(b)** Pie charts showing the trap size distribution depending on their structure, in black the proportion of IA and in grey the proportion of CA. The checkboards pattern represents all traps exhibiting a diameter $D > 4\mu\text{m}$ (large traps).

Using optical microscopy at a magnification of $\times 100$, which possesses a lower resolution compared to X-ray tomography, only larger traps are visible. Microfluidic observations realized with an optical microscope have shown that trapping only occurred on visible traps, i.e. larger traps, that originate for 90 % of them from CA structure. This is consistent with the fact that this structure is expected to be more efficient, taking benefit of its high aspect ratio which favors the concentration of magnetic field lines (Khashan and Furlani 2014). Considering that (i) the density of traps is of first importance in the trapping capacity of the device, and (ii) larger traps are the efficient ones, we focused our attention on the characterization of the population of large traps, 4 to 11 μm in diameter, of 5 wt% sample. Their density reaches 1300 traps/ mm^2 with nearest neighbour distances center-to-center ranging from 17 to 27 μm as reported on Fig. 5. This trapping array specification suits for our beads models (12 μm diameter) but also for larger target such as WBCs, or cells.

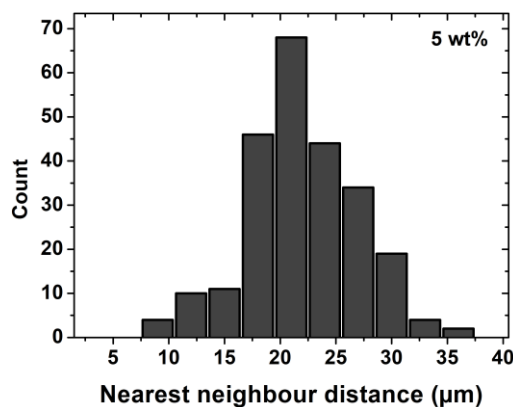


Fig. 5 Nearest neighbour distances, center-to-center, for large traps (diameter $> 4\mu\text{m}$) of 5 wt% composite

3.2 Trapping characterization in microfluidic channel

In our experimental set-up, the microfluidic device is positioned on a NdFeB magnet that generates a 300 mT magnetic field in the channel, i.e. at 2 mm from the magnet surface. From

COMSOL® simulations, we expect a 18.2 T/m magnetic field gradient originating from the magnet underneath the device. In order to estimate the effect of the magnet alone, we first carried out a series of experiments without magnetic composite. We observed an average of only 3 immobilized beads in frame at 500 $\mu\text{L}/\text{h}$ and none at 1 mL/h, on pure PDMS floor. This reference series of experiment ensures that in the following study, the trapping can be attributed to the composite membrane.

The 5 wt% membrane was then implemented into microfluidic devices, constituting the bottom side of a microfluidic channel (Fig. 1j). The trapping area was 1 mm large (channel width) and 1 cm long. Superparamagnetic beads were injected in the device with flow rate ranging between 1 to 3.5 mL/h, corresponding to flow velocities ranging between 2.8 to 9.7 mm/s. For flow rates below 3 mL/h, all beads were trapped (100% trapping efficiency), individually or in clusters, during the gradual filling of the trapping area. The supplemental bead injection optimized the filling of the traps but also favored the formation of bead clusters.

For flow rate of 3 mL/h, few un-trapped beads were observed during the progressive filling of traps. We therefore studied the trapping characteristics of the device at the optimum flow rates of 3 and 3.5 mL/h. We timed the experiments until beads reached the end of the trapping area and then we stopped the flow. Fig. 6 a) reports a microscopic image of the traps in the channel before and after trapping of the beads once the flow was stopped. During experiments un-trapped beads were counted in order to determine trapping efficiency. Table 1 shows the trapping efficiency, throughput, density of trapped beads, and ratio of traps occupied by one single beads, at 3 and 3.5 mL/h.

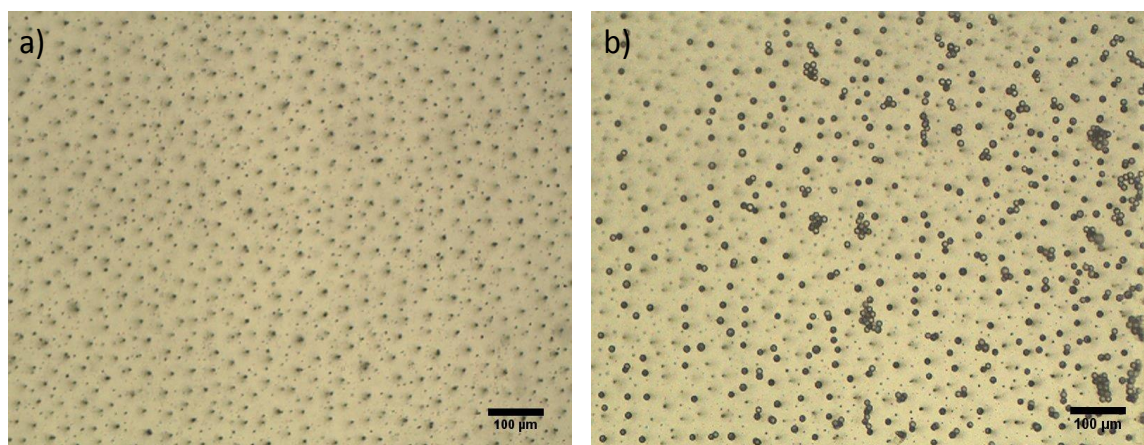


Fig. 6 Microscopic images of the trapping area (a) before and (b) after capture of the beads at a flow velocity of 9.8 mm/s (3.5 mL/h).

The trapping efficiency of the device was found to be very high, in the order of 99.99%. Experiments lasted 1 min and few seconds, and 7950 beads (750 beads/ mm^2) and 5646 beads (646 beads/ mm^2) were trapped at respectively 3 and 3.5 mL/h. Average throughput of 7100 trapped beads/min and 4733 trapped beads/min were calculated. These performances compete with the one reported for hydrodynamic approaches (Narayanamurthy et al. 2017).

Table 1 Composite membrane trapping characteristics: throughput, trapping efficiency, number and density of trapped beads, ratio of traps occupied with a single bead, at flow rate of 3 and 3.5 mL/h, which correspond to flow velocities of 8.3 and 9.7 mm/s.

Flow rate mL/h	Velocity mm/s	Throughput beads/min	Trapping efficiency	Number of trapped beads	Density Beads/mm ²	Traps with single bead
3	8.3	7100 +/- 500	99.99 %	7951 +/- 562	750 +/- 57	28 %
3.5	9.7	4733 +/- 338	99.99 %	5646 +/- 413	656 +/- 41	46.7 %

The trapping dynamics in the channel can be describe as follows. The first beads were captured on traps at the beginning of the trapping area and homogeneously across the channel width. The gradual filling of traps appeared heterogenous along the trapping area. Indeed, an average of 25% of the traps are occupied by single beads or clusters of beads in the total area, but 41% at its entrance and 5% at its end. Fig. 7 reports the number of trapped beads at different positions in the channel. The dimensions of each observation window are 750 μm long and 1000 μm width, which corresponds to the channel width, they are numbered form N1 to N5, as represented on Fig. 7(a). For a flow velocity of 8.3 mm/s (flow rate of 3 mL/h), the number of trapped beads decreases from 1085 (13.6% of the total of trapped beads) in N1, to 591 (7.4 %) in N3 to 150 (1.9 %) in N5.

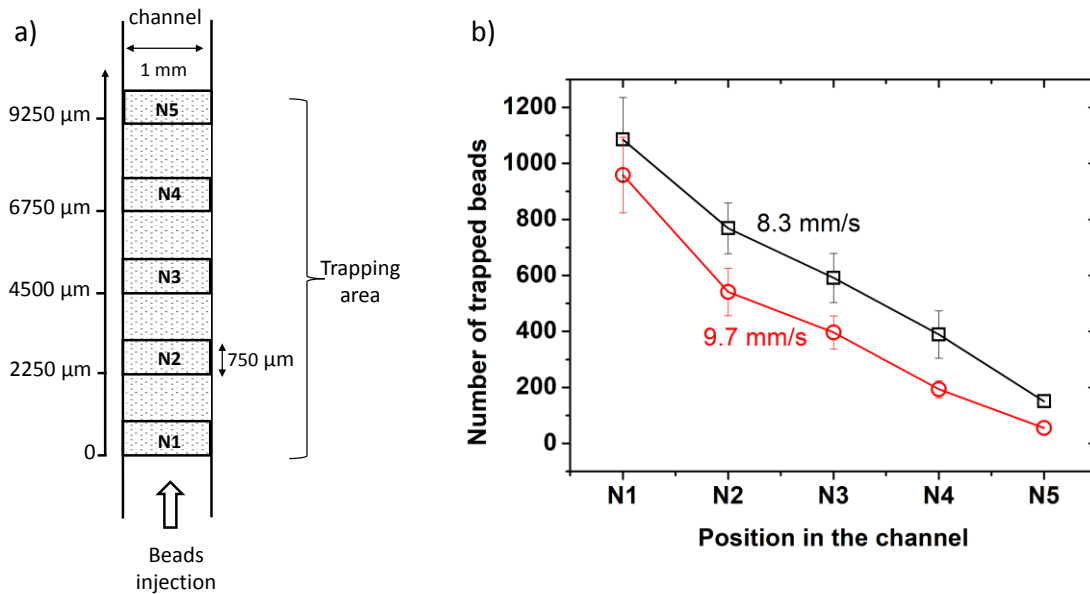


Fig. 7 (a) Schematic representation of observation windows, N1, N2, N3, N4 and N5, positioned at 0 μm , 2250 μm , 4500 μm , 6750 μm , 9250 μm from the entrance of the trapping area, **(b)** number of trapped beads in the channel in each observation window.

Besides trapping dynamic, these arrays of magnetic structures could be used to immobilize single objects, notably for assays on large populations of individual cells. In this view, we put the focus on the fraction of single beads occupying traps. With flow velocities of 8.3 mm/s and 9.7 mm/s, 28 % and 46.7 % of the traps were occupied by a single bead, the others by bead clusters, as reported on Table 1. The higher fraction of single beads at 9.7 mm/s than at 8.3 mm/s could be attributed to the relatively small cohesion of bead clusters, as expected from dipolar interactions between superparamagnetic beads, and that the formation of the clusters is

essentially due to bead-trap interactions. Fig. 8 reports the ratio of traps occupied by a single bead. This ratio exceeds 50 % in the middle of trapping area at 9.7 mm/s, whereas it remains lower than 32 % at 8.3 mm/s.

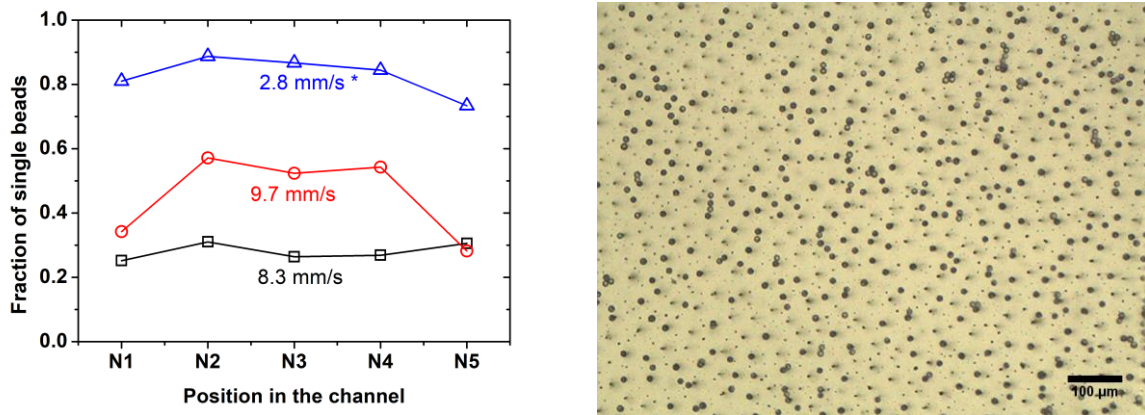


Fig. 8 (a) Fraction of filled traps with a single bead for flow velocities of 8.3 mm/s, 9.7 mm/s and 2.8 mm/s followed by short accelerations. **(b)** Microscopic images of the trapping area after single bead trapping optimization (and 2.8 mm/s followed by short accelerations)

The low cohesion of bead clusters permits to foresee different routes to increase the number of individual trapped beads in the device, notably by modulating the flow rate in time. To illustrate it, we injected beads in the device at lower flow rate, 1 mL/h (flow velocity of 2.8 mm/s), in order to fill the entire trapping zone with beads and clusters. Then, to break beads clusters, we created short acceleration through pressure drop by moving capillary. Fig. 8 (b) reports a microscopic image of beads trapping in the device. One can observe the absence of large beads clusters and a larger proportion of single bead trapped. As reported on Fig. 8, the traps occupied by a single bead represent 73 % to 88 % of occupied traps. A better control of the short accelerations could permit to precisely monitor the coverage of the microbead array.

4 Conclusion

In this paper, we propose a novel technology to obtain efficient magnetic micro-traps. This novel technology, inspired by composite-polymer approach, is low cost and requires simple fabrication process that break with standard microfabrication processes. Developed microtraps consist of chains of Fe-C microparticles diluted in the PDMS. X-ray tomography experiments gave significantly better insights of microstructure engineering mechanisms for low Fe-C concentration magnetic composites (1 wt% and 5wt%). The self-organization of Fe-C particles in a PDMS matrix leads to the creation of highly dense arrays of chain-like agglomerates in large proportion, together with sparse isotropic small agglomerates. Larger traps, originated for 90% of them from CA structure, were identified as the most efficient ones. Their density reached 1300 magnetic microtraps/mm², with diameter from 4 to 11 μm, and an average nearest neighbour distance of 21 μm. They were implemented in a microfluidic channel. We assessed the trapping efficiency and throughput of the device and studied the trapping dynamics. We obtained trapping efficiency of 99,99% at flow velocities of 8.3 to 9.7 mm/s. At 8.3 mm/s, throughputs up to 7100 trapped beads/min were measured. At 9,7 mm/s the ratio on single bead traps was improved. This novel technology allows to trap thousands of beads with throughputs that, to the best of our knowledge, were never reported using magnetic forces and that permit to compete with hydrodynamic trapping functions, while requiring simple fabrication process, and handling.

1
2 **Acknowledgements**
3

4 We wish to acknowledge support for the project from Ecole doctorale EEA and regional AURA
5 financial support, Nanolyon technological platform, MATEIS lab for X-ray tomography
6 analyses, and A. Piednoir for AFM characterization at ILM.
7

8
9 **References**

10
11 Arnold DP, Wang N (2009) Permanent magnets for MEMS. *J Microelectromechanical Syst*
12 18:1255–1266
13

14 Cetin B, Özer MB, Solmaz ME (2014) Microfluidic bio-particle manipulation for
15 biotechnology. *Biochem Eng J* 92:63–82
16

17
18 Chen H, Sun J, Wolvetang E, Cooper-White J (2015) High-throughput, deterministic single
19 cell trapping and long-term clonal cell culture in microfluidic devices. *Lab Chip* 15:1072–
20 1083
21

22
23 Chen P, Huang Y-Y, Hoshino K, Zhang X (2014) Multiscale immunomagnetic enrichment of
24 circulating tumor cells: from tubes to microchips. *Lab Chip* 14:446–458
25

26 Delapierre F-D, Mottet G, Taniga V, et al (2017) High throughput micropatterning of
27 interspersed cell arrays using capillary assembly. *Biofabrication* 9:015015
28

29 Deman A-L, Chateaux J-F, Dhungana D, et al (2017) Anisotropic composite polymer for high
30 magnetic forces in microfluidic systems. *Microfluid. Nanofluidics*
31

32
33 Dempsey NM, Le Roy D, Marelli-Mathevon H, et al (2014) Micro-magnetic imprinting of
34 high field gradient magnetic flux sources. *Appl Phys Lett* 104:262401
35

36
37 Dempsey NM, Walther A, May F, et al (2007) High performance hard magnetic NdFeB thick
38 films for integration into micro-electro-mechanical systems. *Appl Phys Lett* 90:092509
39

40 Dumas-Bouchiat F, Zanini L-F, Kustov M, et al (2010) Thermomagnetically patterned
41 micromagnets. *Appl Phys Lett* 96:102511
42

43
44 Esmaeilsabzali H, Beischlag TV, Cox ME, et al (2016) An integrated microfluidic chip for
45 immunomagnetic detection and isolation of rare prostate cancer cells from blood. *Biomed*
46 *Microdevices* 18:22
47

48
49 Faivre M, Gelszinnis R, Degouttes J, et al (2014) Magnetophoretic manipulation in
50 microsystem using carbonyl iron-polydimethylsiloxane microstructures. *Biomicrofluidics*
51 8:054103
52

53 Forbes TP, Forry SP (2012) Microfluidic magnetophoretic separations of
54 immunomagnetically labeled rare mammalian cells. *Lab Chip* 12:1471–1479
55

56
57 Ghosh S, Puri IK (2013) Soft polymer magnetic nanocomposites: microstructure patterning
58 by magnetophoretic transport and self-assembly. *Soft Matter* 9:2024–2029
59
60
61
62
63
64
65

1 Günther D, Borin DY, Günther S, Odenbach S (2011) X-ray micro-tomographic
2 characterization of field-structured magnetorheological elastomers. *Smart Mater Struct*
3 21:015005

4 Henighan T, Chen A, Vieira G, et al (2010) Manipulation of magnetically labeled and
5 unlabeled cells with mobile magnetic traps. *Biophys J* 98:412–417

6
7
8 Hosis S, Murthy SK, Koppes AN (2015) Microfluidic sample preparation for single cell
9 analysis. *Anal Chem* 88:354–380

10
11 Jaiswal D, Rad AT, Nieh M-P, et al (2017) Micromagnetic cancer cell immobilization and
12 release for real-time single cell analysis. *J Magn Mater* 427:7–13

13
14
15 Jung Y, Choi Y, Han K-H, Frazier AB (2010) Six-stage cascade paramagnetic mode
16 magnetophoretic separation system for human blood samples. *Biomed Microdevices* 12:637–
17 645

18
19
20 Khashan SA, Furlani EP (2014) Scalability analysis of magnetic bead separation in a
21 microchannel with an array of soft magnetic elements in a uniform magnetic field. *Sep Purif*
22 *Technol* 125:311–318

23
24
25 Kim H, Lee S, Kim J (2012) Hydrodynamic trap-and-release of single particles using dual-
26 function elastomeric valves: design, fabrication, and characterization. *Microfluid Nanofluidics*
27 13:835–844

28
29 Le Roy D, Dhungana D, Ourry L, et al (2016a) Anisotropic ferromagnetic polymer: A first
30 step for their implementation in microfluidic systems. *AIP Adv* 6:056604

31
32
33 Le Roy D, Shaw G, Haettel R, et al (2016b) Fabrication and characterization of polymer
34 membranes with integrated arrays of high performance micro-magnets. *Mater Today*
35 *Commun* 6:50–55

36
37
38 Li J, Zhang M, Wang L, et al (2011) Design and fabrication of microfluidic mixer from
39 carbonyl iron–PDMS composite membrane. *Microfluid Nanofluidics* 10:919–925

40
41 Marchi S, Casu A, Bertora F, et al (2015) Highly magneto-responsive elastomeric films
42 created by a two-step fabrication process. *ACS Appl Mater Interfaces* 7:19112–19118

43
44
45 Mohamadi RM, Besant JD, Mephram A, et al (2015) Nanoparticle-Mediated Binning and
46 Profiling of Heterogeneous Circulating Tumor Cell Subpopulations. *Angew Chem* 127:141–
47 145

48
49
50 Nam J, Huang H, Lim H, et al (2013) Magnetic separation of malaria-infected red blood cells
51 in various developmental stages. *Anal Chem* 85:7316–7323

52
53
54 Narayanamurthy V, Nagarajan S, Samsuri F, Sridhar T (2017) Microfluidic hydrodynamic
55 trapping for single cell analysis: mechanisms, methods and applications. *Anal Methods*
56 9:3751–3772

57
58
59 Rampini S, Li P, Lee G (2016) Micromagnet arrays enable precise manipulation of individual
60 biological analyte–superparamagnetic bead complexes for separation and sensing. *Lab Chip*
61 16:3645–3663

62
63
64
65

1 Rasponi M, Piraino F, Sadr N, et al (2011) Reliable magnetic reversible assembly of complex
2 microfluidic devices: fabrication, characterization, and biological validation. *Microfluid*
3 *Nanofluidics* 10:1097–1107

4 Royet D, Hériveaux Y, Marchalot J, et al (2017) Using injection molding and reversible
5 bonding for easy fabrication of magnetic cell trapping and sorting devices. *J Magn Mater*
6 *427*:306–313

7
8
9 Saliba A-E, Saias L, Psychari E, et al (2010) Microfluidic sorting and multimodal typing of
10 cancer cells in self-assembled magnetic arrays. *Proc Natl Acad Sci* 107:14524–14529

11
12 Tekin HC, Gijs MA (2013) Ultrasensitive protein detection: a case for microfluidic magnetic
13 bead-based assays. *Lab Chip* 13:4711–4739

14
15
16 Xu X, Li Z, Kotagiri N, et al (2013) Microfluidic microsphere-trap arrays for simultaneous
17 detection of multiple targets. *International Society for Optics and Photonics*, p 86151E

18
19 Yesilkoy F, Ueno R, Desbiolles B, et al (2016) Highly efficient and gentle trapping of single
20 cells in large microfluidic arrays for time-lapse experiments. *Biomicrofluidics* 10:014120

21
22
23 Yu X, Feng X, Hu J, et al (2011) Controlling the magnetic field distribution on the
24 micrometer scale and generation of magnetic bead patterns for microfluidic applications.
25 *Langmuir* 27:5147–5156

26
27
28 Zanini L-F, Dempsey NM, Givord D, et al (2011) Autonomous micro-magnet based systems
29 for highly efficient magnetic separation. *Appl Phys Lett* 99:232504

30
31 Zhou R, Wang C (2016) Microfluidic separation of magnetic particles with soft magnetic
32 microstructures. *Microfluid Nanofluidics* 20:48